Spillover of active oxygen intermediates of binary RuO_2/Nb_2O_5 nanowires for highly active and robust acidic oxygen evolution

Linqing Liao,[#ab] Wangyan Gou,[#c] Mingkai Zhang,[d] Xiaohe Tan,[ab] Zening Qi,[e] Min Xie,[e] Yuanyuan Ma*[ab] and Yongquan Qu*[ab]

[a] *Research & Development Institute of Northwestern Polytechnical University in Shenzhen, Shenzhen, 518057, China. E-mail: yyma@nwpu.edu.cn ; yongquan@nwpu.edu.cn*

[b] *Key Laboratory of Special Functional and Smart Polymer Materials of Ministry of Industry and Information Technology, School of Chemistry and Chemical Engineering, Northwestern Polytechnical University, Xi'an, 710072, China.*

[c] *School of Materials Engineering, Xi'an Aeronautical University, Xi'an, 710077, China*

[d] *School of Science Xi'an University of Technology Xi'an, 710048, China*

[e] *Xi'an Yiwei Putai Environmental Protection Co., LTD, Xi'an, 710065, China*

[#] *These authors contributed equally to this study.*

Experimental details

Materials

Ruthenium (III) chloride trihydrate ($RuCl_3 \cdot 3H_2O$), N, N-dimethylformamide (DMF) and sulfuric acid (H_2SO_4) were bought from Energy Chemical. Ruthenium (IV) oxide (RuO_2), Nafion 117 solution (5 wt%), methanol, and polyvinylpyrrolidone (PVP, MW = 1300000) were purchased from Sigma-Aldrich.

Synthesis of RuO_2/Nb_2O_5-x

In this paper, the stoichiometric ratio of the catalysts was modulated by the molecular ratio of initial metal precursors, labeled as RuO_2/Nb_2O_5-x (x = n/0.4, n = mole number of Ru). If not specifically labeled, the sintering temperature was 400℃. RuO_2/Nb_2O_5 nanotubes were prepared by electrospinning and calcination method. 400 mg of polyvinylpyrrolidone (PVP, MW = 1300000) was dissolved in 1.6 mL of N, N-dimethylformamide (DMF). The solution was placed on a magnetic stirrer and maintained for 12 h.

Niobium chloride ($NbCl_5$) and ruthenium chloride trihydrate ($RuCl_3\ 3H_2O$) were proportionally weighed with the total amount of 0.4 mmol. $NbCl_5$ was dissolved in 500 μL of anhydrous ethanol and $RuCl_3 \cdot 3H_2O$ was dissolved in 800 μL of DMF, respectively, and each of them was separately sonicated for 15 min. Afterwards, the ruthenium chloride solution was dropped into the PVP solution, followed by the addition of niobium chloride. The mixture was placed under vigorous stirring for 8 h and kept standing for 12 h to remove bubbles.

Next, the precursor solution was added into a plastic syringe and electrospun with an electrostatic spinner at a flow rate of 12 mL/h and a voltage of 13 kV. The precursor was heated up to a predetermined temperature (300℃, 400℃, 500℃) in a tube furnace with a ramping rate of 5 ℃/min and maintained for 6 h in air atmosphere, and then cooled naturally to room temperature. The RuO_2/Nb_2O_5-x were prepared. RuO_2 nanowires were synthesized in the same way without the addition of niobium chloride.

Material characterization

X-ray Diffraction (XRD) was performed by a Bruker D8 Advance with an operating voltage of 30 kV and an operating current of 20 mA. Scan rate was 2 °/min. Transmission electron microscopy (TEM) was performed on JEOL JEM-F200 transmission electron microscope at 200 kV, respectively. X-ray photoelectron spectroscopy (XPS) was tested by Thermo Scientific K-Alpha. The test results were corrected with reference to the C 1s peak (284.8 eV). Raman spectra were tested using an INVIAREFLEX Raman spectrometer with an excitation wavelength of 633 nm.

Electrochemical measurements

The catalyst ink containing 4 mg of prepared sample, 768 μL of ultrapure water, 200 μL of anhydrous ethanol and 32 μL of Nafion 117 were prepared through extensive sonication. The prepared slurry was pipetted to form droplets with 3 mm diameter by dropping 10 μL onto carbon paper (1 cm × 3 cm) and dried naturally. The electrochemical test system was a three-electrode system, in which the electrolyte was

0.5 M H_2SO_4, the working electrode was carbon paper with loading material, the reference electrode was $Hg/Hg_2Cl_2/KCl$ electrode, and the counter electrode was graphite sheet electrode.

According to the equation:

$$E(versus\ RHE) = E(versus\ Hg\ /\ HgO) + 0.241\ V + \ 0.059\ V\ \times pH$$

All measured potentials in this document were calibrated to the reversible hydrogen electrode (RHE) potential. Linear scanning voltametric curves (LSV) were tested at a scan rate of 10 mV s^{-1}. The linear part of the Tafel plot was simulated polarization curve by the Tafel equation ($\eta = \ b\ log[i] + a$) to obtain the Tafel slope. The turnover frequency (TOF) was calculated by TOF = (j × A)/(4 × F × n), where j was the current density (mA cm^{-2}) at a particular overpotential, A was the area (cm^{-2}) of the working electrode, F was the Faraday constant (96,500 C mol^{-1}), and n was the number of moles of the active materials. The mass activity could be calculated by mass activity = j/m, where m was the mass loading of Ru in the working electrode (mg cm^{-2}) and j was the measured current density (mA cm^{-2}) at given potential. The S-numbers ($S = n_{O2}/n_{Ru}$) of various catalysts at 10 mA cm^{-2} were calculated. The CV curves at different scan rates (10 mV s^{-1}-60 mV s^{-1}) were linearly fitted to obtain C_{dl}, and the electrochemically active surface area (ECSA) was obtained by further calculations ($ECSA=C_{dl}/C_s$, C_s=0.06 mF/cm^2).

In situ **attenuated total reflectance-surface-enhanced infrared absorption spectra (ATR-SEIRAS).** The ATR-SEIRAS experiments were carried out by a Nicolet

iS50 FT-IR spectrometer equipped with a chemically deposited ultra-thin Au film as working electrode for infrared signal enhancement. The catalyst slurry was dripped onto carbon paper and then connected to the working electrode after drying, while saturated $Hg/Hg_2Cl_2/KCl$ electrode and graphite rod served as reference electrode and counter electrode, respectively. *In situ* ATR-SEIRAS signals were recorded when the electrodes were under potentiostatic tests.

***In situ* Raman spectrometry measurements.** *In situ* Raman measurements were carried out jointly by an inVia-Reflex (Renishaw, 633 nm) and a CHI 760 electrochemical workstation. A homemade Teflon cell with a quartz window was used as the reactor for the *in-situ* measurements. The obtained electrodes, $Hg/Hg_2Cl_2/KCl$ electrode, and platinum wire served as the working electrode, reference electrode, and counter electrode, respectively. The working electrode was immersed into the electrolyte with different configurations and the electrode plane was maintained perpendicular to the laser. In situ Raman spectra were obtained when the electrodes were under potentiostatic control. The experiments were controlled within 300 s under the fixed potential.

Table. S1. ICP-ES analysis of RuO_2/Nb_2O_5-0.5, RuO_2/Nb_2O_5-0.6 and RuO_2/Nb_2O_5-0.7.

Sample	Ru loading(wt%)	Nb loading(wt%)	Molar ratio of Ru:(Ru+Nb)
RuO_2/Nb_2O_5-0.5	12.32%	11.15%	0.50
RuO_2/Nb_2O_5-0.6	25.69%	16.20%	0.59
RuO_2/Nb_2O_5-0.7	15.68%	6.45%	0.69

Table S2. Quantitative analysis of RuO_2/Nb_2O_5-0.6 by energy-dispersive X-ray spectroscopy.

Element	(keV)	Mass%	Atom%
O K (Ref.)	0.525	25.48	67.70
Nb L	2.166	26.08	11.93
Ru L	2.558	48.44	20.37
Total	-	100.00	100.00

Table. S3. Comparison of activity and stability of OER with previous reports.

Entry	Catalyst	Overpotential (η_0) at 10 mA cm^{-2} [mV]	Stability at 10 mA cm^{-2}[h]	Reference
	RuO_2/Nb_2O_5-0.6	**179**	**750**	**This work**
1	$(Ru, Mn)_2O_3$	168	40	Ref. 1
2	IrCuNi	273	-	Ref. 2
3	Ir/Nb_2O_5	218	105	Ref. 3
4	IrO_x/Ti	254	100	Ref. 4
5	Ni-RuO_2	214	>200	Ref. 5
6	RuO_2/D-TiO_2	180	100	Ref. 6
7	$Li_{0.52}RuO_2$	156	70	Ref. 7
8	SF-RuO_2	196	24	Ref. 8
9	$Sn_{0.1}$-RuO_2@NCP	178	150	Ref. 9
10	RuPbOx	196	100	Ref. 10
11	$Ru_1Ir_1O_x$	204	110	Ref. 11
12	SrRuIr	190	1500	Ref. 12
13	C-RuO_2-RuSe-5	212	50	Ref. 13
14	Ru(anc)−Co_3O_4	198.5	150	Ref. 14
15	La-RuO_2	208	-	Ref. 15
16	Ru-UiO-67-bpydc	200	115	Ref. 16
17	$Nd_{0.1}RuO_x$	211	50	Ref. 17
18	M-RuIrFeCoNiO_2	189	120	Ref. 18

Table S4. The O_H/O_V of catalysts.

Catalyst	O_H/O_V
RuO_2/Nb_2O_5-0.6	1.49
RuO_2/Nb_2O_5-0.5	0.68
RuO_2/Nb_2O_5-0.7	1.08

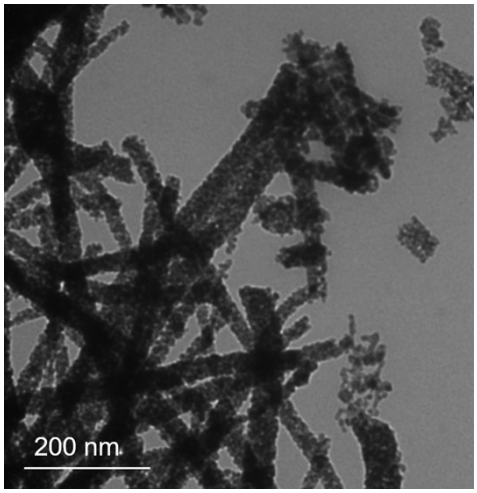

Fig. S1. TEM image of as-synthesized RuO_2.

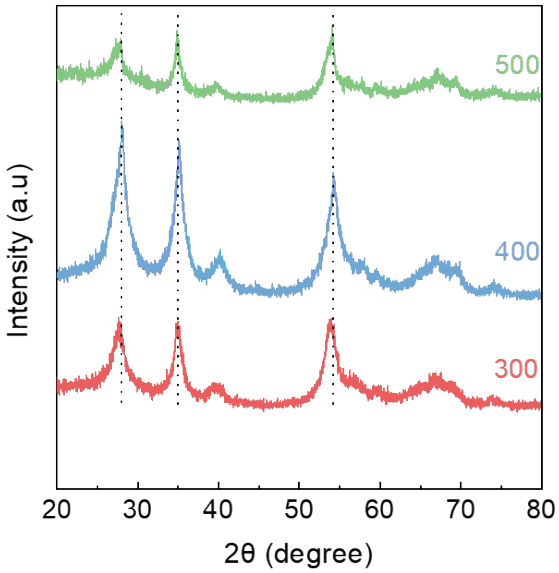

Fig. S2. XRD patterns of RuO_2/Nb_2O_5-0.6 prepared at different calcination temperatures (300℃, 400℃ and 500℃).

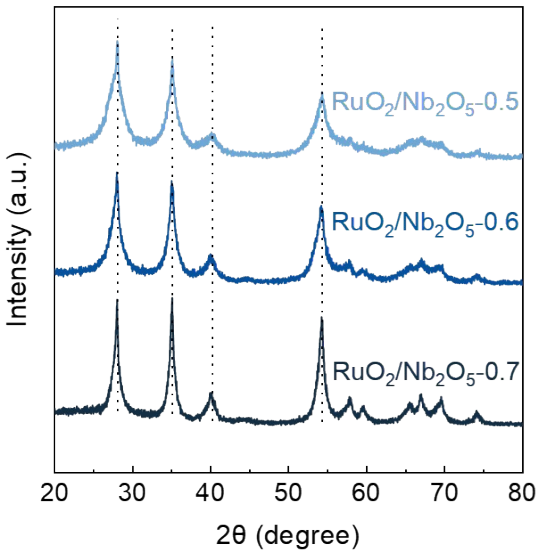

Fig. S3. XRD patterns of RuO_2/Nb_2O_5-x (x=0.5, 0.6, 0.7) synthesized at 400 ℃.

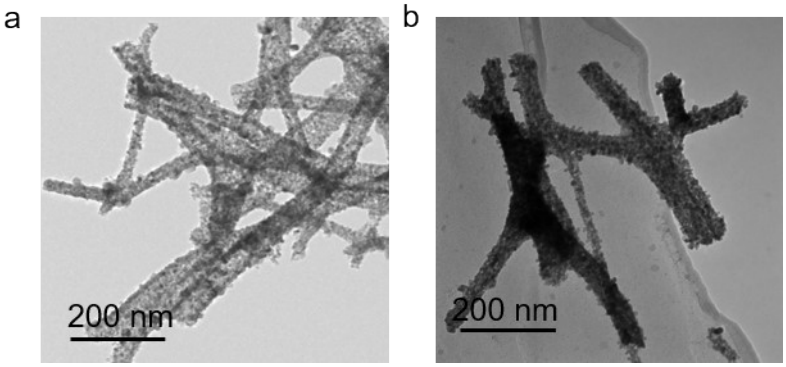

Fig. S4. TEM images of (a) RuO_2/Nb_2O_5-0.7, (b) RuO_2/Nb_2O_5-0.5.

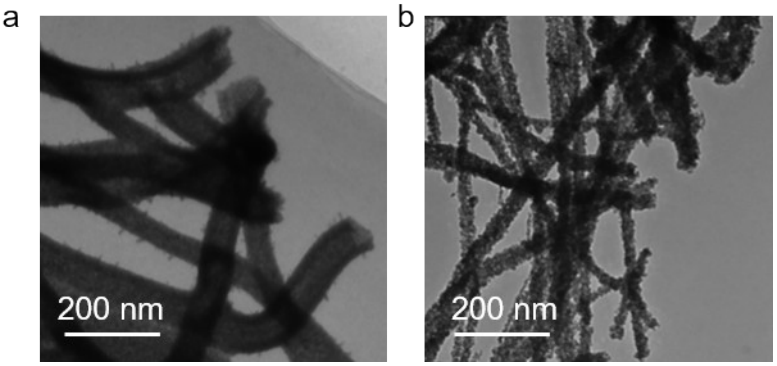

Fig. S5. TEM images of RuO_2/Nb_2O_5-0.6 calcinated at (a) 300℃ and (b) 500℃.

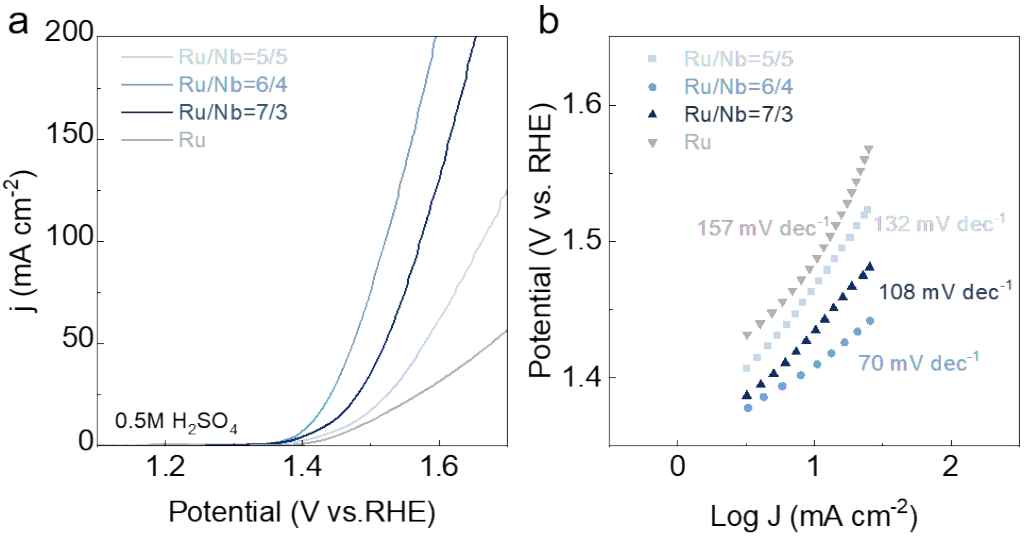

Fig. S6. (a) LSV curves and (b) Tafel slopes of RuO_2/Nb_2O_5-x (x=0.5, 0.6 and 0.7) prepared at 400 ℃ in 0.5 M H_2SO_4 solution.

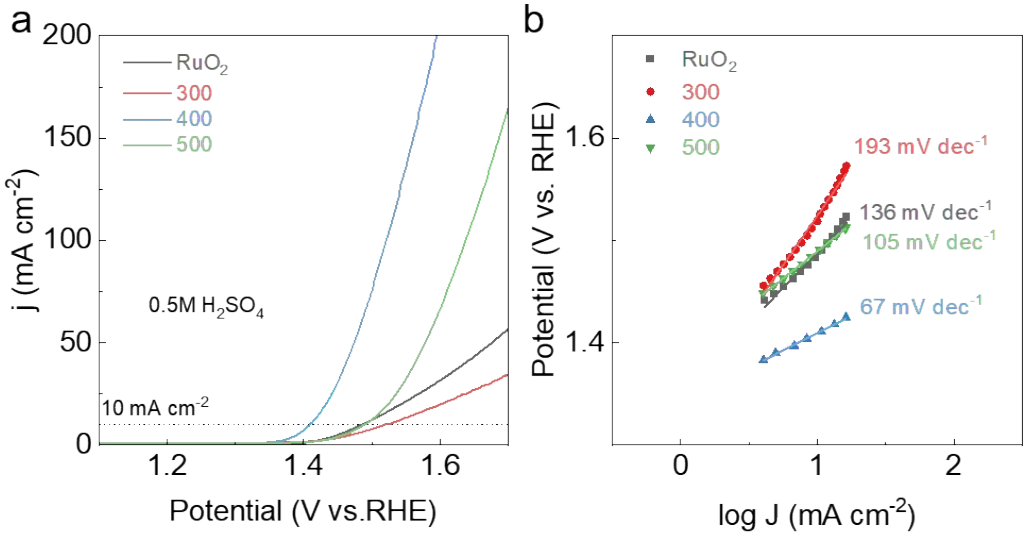

Fig. S7. (a) LSV curves and (b) Tafel slopes of RuO_2/Nb_2O_5-0.6 calcinated at 300℃, 400℃ and 500℃ in 0.5 M H_2SO_4 solution.

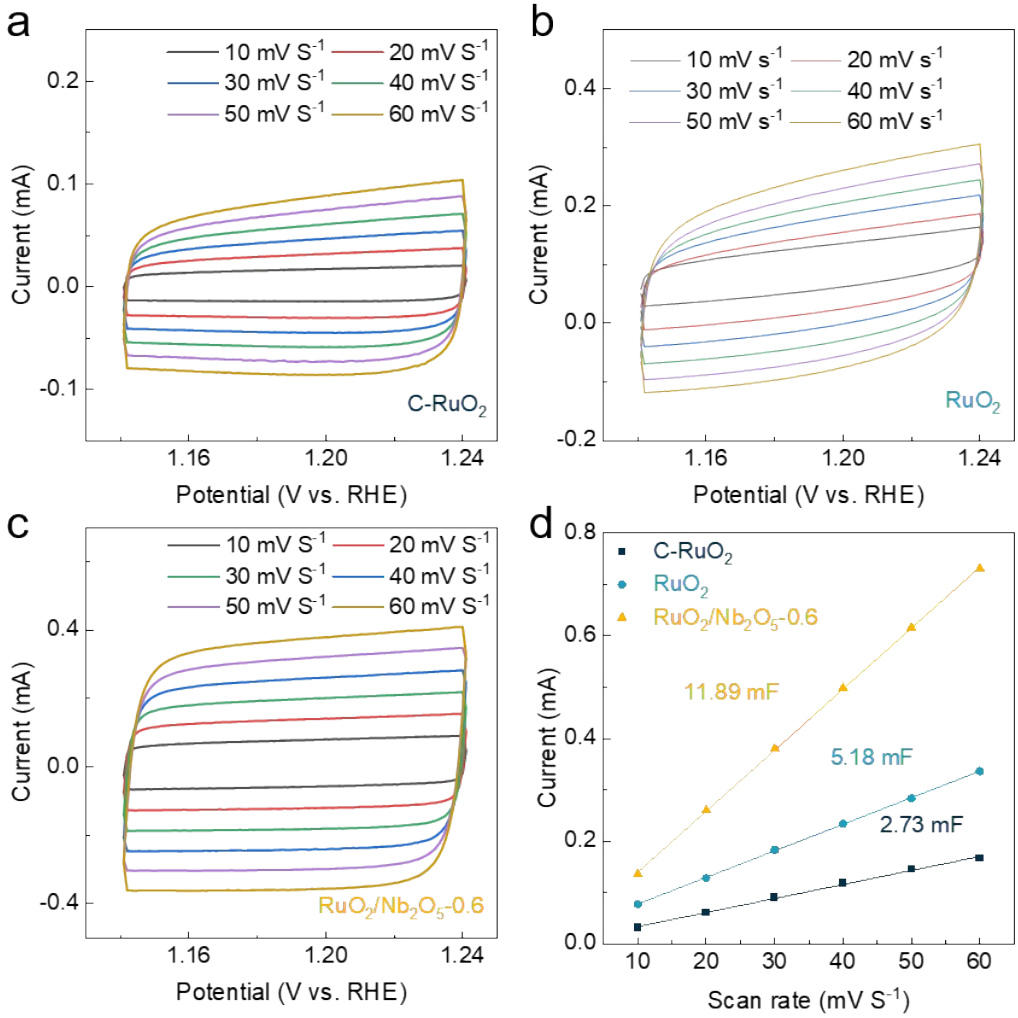

Fig. S8. CV curves of (a) C-RuO_2, (b) RuO_2, (c) RuO_2/Nb_2O_5-0.6 at different scan rates. (d) Charging currents differences plotted versus scan rates.

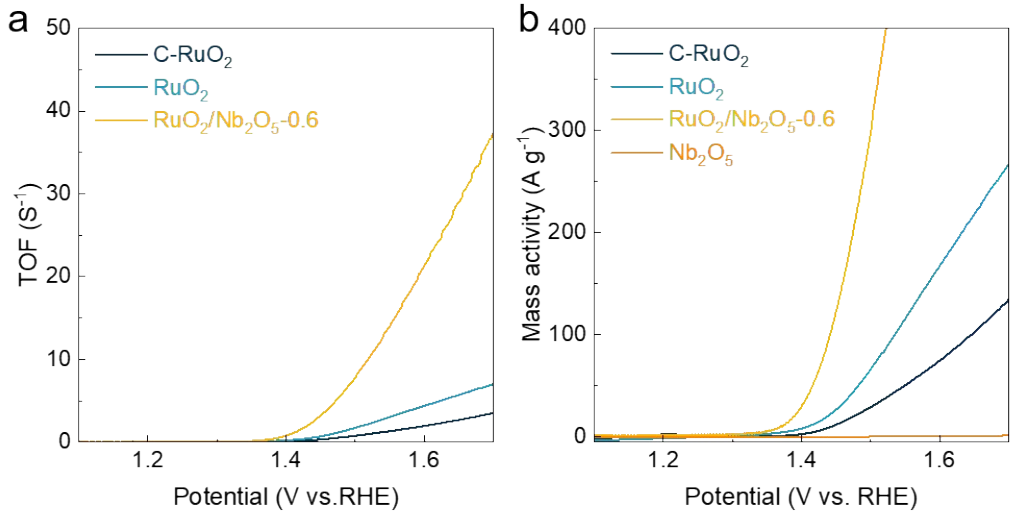

Fig. S9. (a) TOFs and (b) mass activities of various electrocatalysts**.**

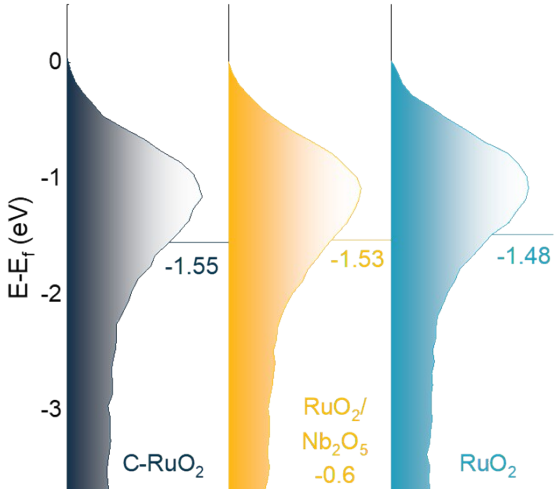

Fig. S10. The d-band of RuO_2/Nb_2O_5-0.6, RuO_2, C-RuO_2 catalysts determined by high-resolution valence-band (VB) XPS spectra.

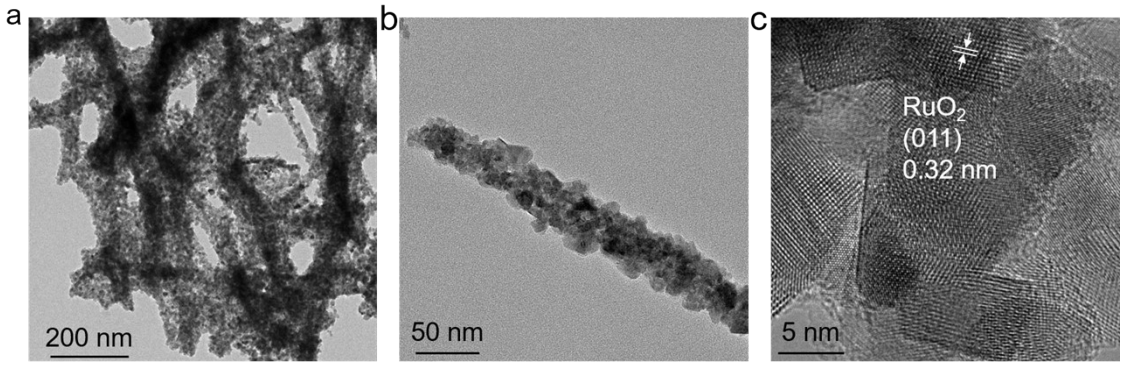

Fig. S11. (a) Low magnification and (b) high magnification TEM images of RuO_2/Nb_2O_5-0.6. (c) HRTEM image of RuO_2/Nb_2O_5-0.6 after stability test.

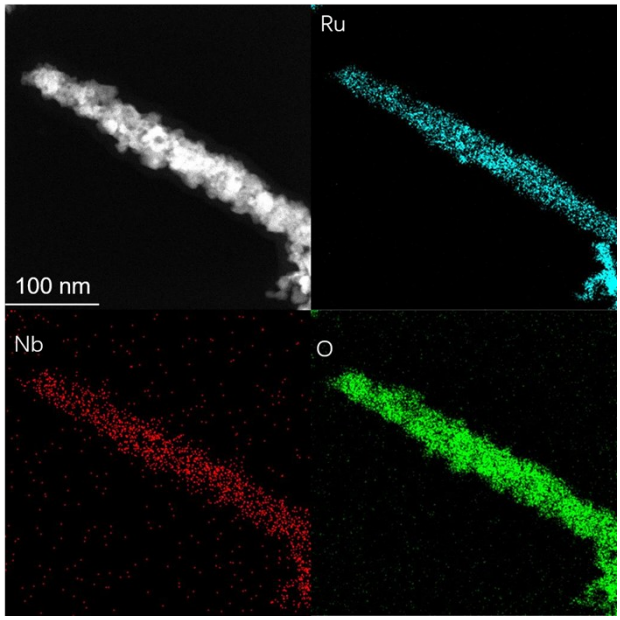

Fig. S12. Elemental mapping images of Ru (blue), Nb (red), and O (green) in RuO_2/Nb_2O_5-0.6 after stability test.

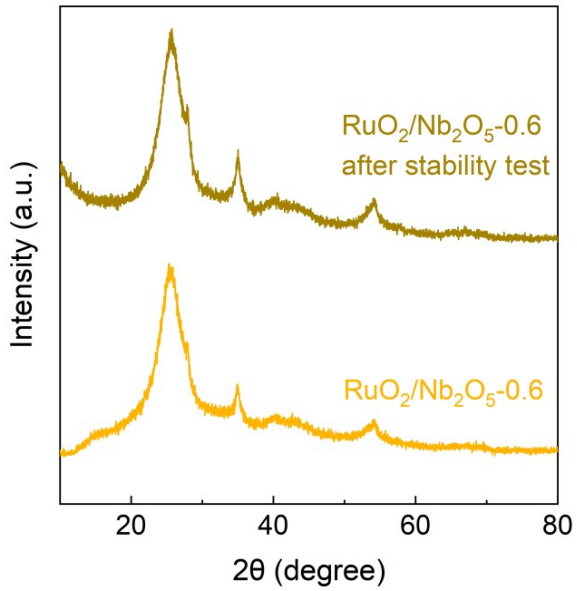

Fig. S13. XRD patterns of as-synthesized and spent RuO_2/Nb_2O_5-0.6 catalysts.

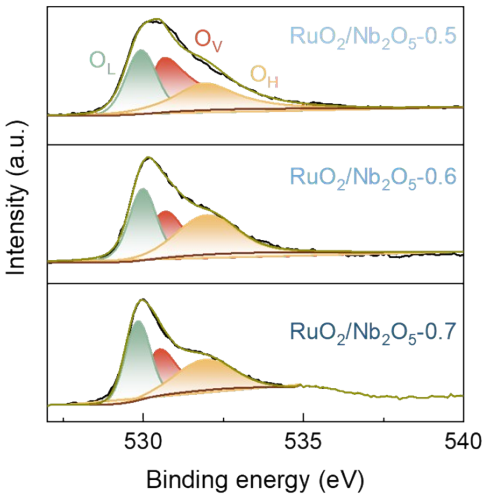

Fig. S14. The O 1s XPS spectra of RuO_2/Nb_2O_5-0.5, RuO_2/Nb_2O_5-0.6 and RuO_2/Nb_2O_5-0.7.

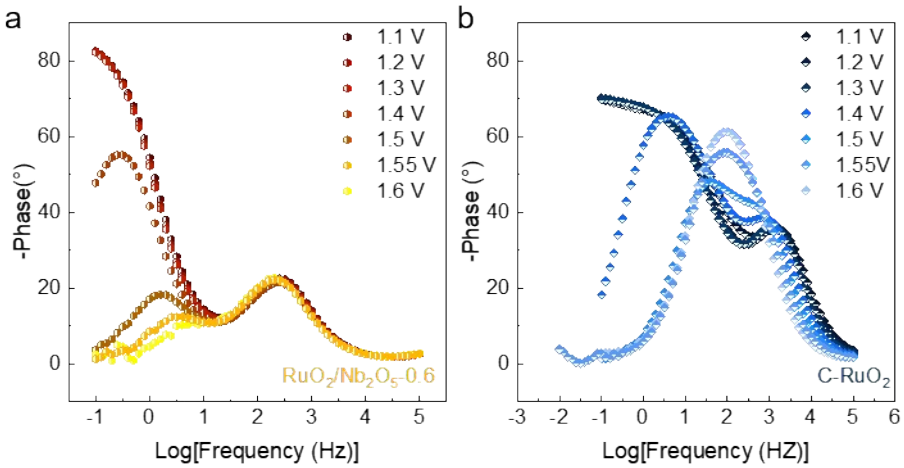

Fig. S15. Bode phase plots of (a) RuO_2/Nb_2O_5-0.6, (b) C-RuO_2.

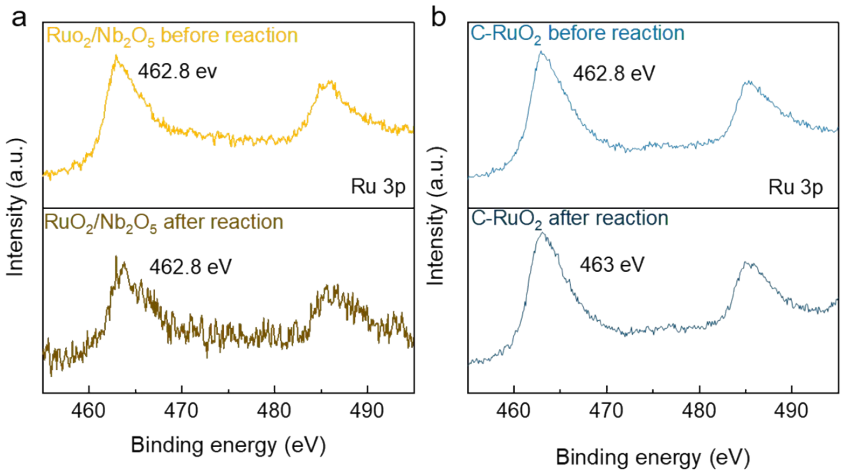

Fig. S16. Ru 3p XPS spectra of (a) RuO_2/Nb_2O_5-0.6 and (b) C-RuO_2 before and after stability test for 10h.

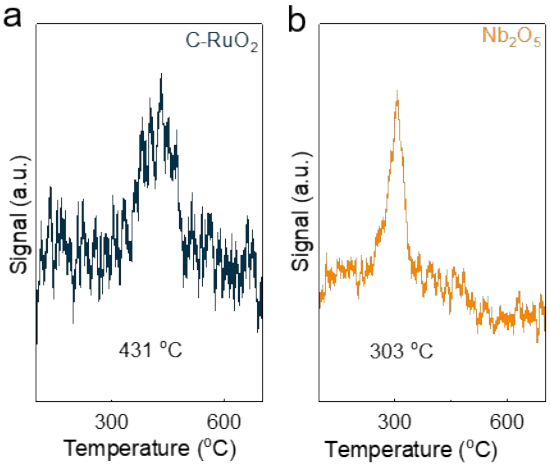

Fig. S17. O_2-TPD profiles of (a) C-RuO_2 and (b) RuO_2/Nb_2O_5-0.6.

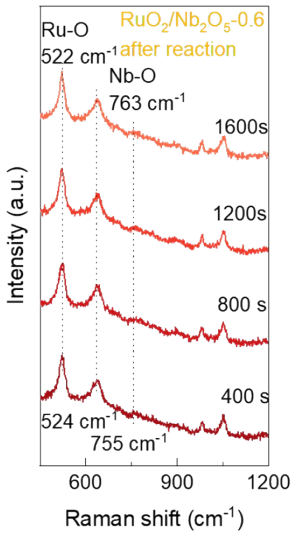

Fig. S18. The operando Raman spectra of RuO_2/Nb_2O_5-0.6 recorded at 400 s, 800 s, 1200 s and 1600 s after reaction with the circuit disconnected.

References

1. Y. Qin, B. Cao, X.-Y. Zhou, Z. Xiao, H. Zhou, Z. Zhao, Y. Weng, J. Lv, Y. Liu, Y.-B. He, F. Kang, K. Li and T.-Y. Zhang, *Nano Energy*, 2023, **115**, 108727.
2. D. Liu, Q. Lv, S. Lu, J. Fang, Y. Zhang, X. Wang, Y. Xue, W. Zhu and Z. Zhuang, *Nano Lett.*, 2021, **21**, 2809-2816.
3. Z. Shi, J. Li, J. Jiang, Y. Wang, X. Wang, Y. Li, L. Yang, Y. Chu, J. Bai, J. Yang, J. Ni, Y. Wang, L. Zhang, Z. Jiang, C. Liu, J. Ge and W. Xing, *Angew. Chem. Int. Ed.*, 2022, **61**, e202212341.
4. Y. Wang, R. Ma, Z. Shi, H. Wu, S. Hou, Y. Wang, C. Liu, J. Ge and W. Xing, *Chem*, 2023, **9**, 2931-2942.
5. Z.-Y. Wu, F.-Y. Chen, B. Li, S.-W. Yu, Y. Z. Finfrock, D. M. Meira, Q.-Q. Yan, P. Zhu, M.-X. Chen, T.-W. Song, Z. Yin, H.-W. Liang, S. Zhang, G. Wang and H. Wang, *Nat. Mater.*, 2023, **22**, 100-108.
6. X. Wang, X. Wan, X. Qin, C. Chen, X. Qian, Y. Guo, Q. Xu, W.-B. Cai, H. Yang and K. Jiang, *ACS Catal.*, 2022, **12**, 9437-9445.
7. Y. Qin, T. Yu, S. Deng, X.-Y. Zhou, D. Lin, Q. Zhang, Z. Jin, D. Zhang, Y.-B. He, H.-J. Qiu, L. He, F. Kang, K. Li and T.-Y. Zhang, *Nat. Commun.*, 2022, **13**, 3784.
8. R. Jiang, Y. Da, J. Zhang, H. Wu, B. Fan, J. Li, J. Wang, Y. Deng, X. Han and W. Hu, *Appl. Catal. B*, 2022, **316**, 121682.
9. L. Qiu, G. Zheng, Y. He, L. Lei and X. Zhang, *Chem. Eng. J.*, 2021, **409**, 128155.
10. R. Huang, Y. Wen, H. Peng and B. Zhang, *Chinese J. Catal.*, 2022, **43**, 130-138.
11. J. He, X. Zhou, P. Xu and J. Sun, *Adv. Energy Mater.*, 2021, **11**, 2102883.
12. Y. Wen, P. Chen, L. Wang, S. Li, Z. Wang, J. Abed, X. Mao, Y. Min, C. T. Dinh, P. Luna, R. Huang, L. Zhang, L. Wang, L. Wang, R. J. Nielsen, H. Li, T. Zhuang, C. Ke, O. Voznyy, Y. Hu, Y. Li, W. A. Goddard, III, B. Zhang, H. Peng and E. H. Sargent, *J. Am. Chem. Soc.*, 2021, **143**, 6482-6490.
13. J. Wang, C. Cheng, Q. Yuan, H. Yang, F. Meng, Q. Zhang, L. Gu, J. Cao, L. Li, S.-C. Haw, Q. Shao, L. Zhang, T. Cheng, F. Jiao and X. Huang, *Chem*, 2022, **8**, 1673-1687.
14. Y. Hao, S.-F. Hung, W.-J. Zeng, Y. Wang, C. Zhang, C.-H. Kuo, L. Wang, S. Zhao, Y. Zhang, H.-Y. Chen and S. Peng, *J. Am. Chem. Soc.*, 2023, **145**, 23659-23669.
15. Y. Wu, R. Yao, Q. Zhao, J. Li and G. Liu, *Chem. Eng. J.*, 2022, **439**, 135699.
16. N. Yao, H. Jia, J. Zhu, Z. Shi, H. Cong, J. Ge and W. Luo, *Chem*, 2023, **9**, 1882-1896.
17. L. Li, G. Zhang, J. Xu, H. He, B. Wang, Z. Yang and S. Yang, *Adv. Funct. Mater.*, 2023, **33**, 2213304.
18. C. Hu, K. Yue, J. Han, X. Liu, L. Liu, Q. Liu, Q. Kong, C.-W. Pao, Z. Hu, K. Suenaga, D. Su, Q. Zhang, X. Wang, Y. Tan and X. Huang, *Sci. Adv.,* 2023, **9**, eadf9144.